Received: 12 June 2020 | Revised: 10 September 2020 | Accepted: 22 October 2020

DOI: 10.4218/etrij.2020-0242

ORIGINAL ARTICLE

ETRI Journal WILEY

Multi-antenna diversity gain in terrestrial broadcasting receivers on vehicles: A coverage probability perspective

Sungjun Ahn | **Jae-young Lee** | **Bo-Mi Lim** | **Hae-Chan Kwon** | **Namho Hur** | **Sung-Ik Park**

Media Research Division, Electronics and Telecommunications Research Institute, Daejeon, Rep. of Korea

Correspondence
Sung-Ik Park, Media Research Division, Electronics and Telecommunications Research Institute, Daejeon, Rep. of Korea.
Email: psi76@etri.re.kr

Funding information
This work was supported by the Institute of Information & Communications Technology Planning & Evaluation (IITP) grant funded by the Korea government (MSIT), Rep. of Korea (2020-0-00846, Development of Convergence Transmission and Technology for 5G and ATSC 3.0 Networks).

This paper theoretically and empirically explores the reliability gain that can be obtained by installing multiple antennas in on-vehicle broadcasting receivers. Analytical derivations reveal that maximal-ratio-combining-based diversity allows a multi-antenna receiver (MR) to achieve significantly better coverage probability than a single-antenna receiver (SR). In particular, the notable MR gains for low-power reception and high-throughput services are highlighted. We also discuss various aspects of mobile MRs, including geometric coverage, volume of the users served, and impact of receiver velocity. To examine the feasibility of MRs in the real world, extensive field experiments were conducted, particularly with on-air ATSC 3.0 broadcast transmissions. Relying on the celebrated erroneous second ratio criterion, MRs with two and four antennas were verified to achieve notable reliability gains over SRs in practice. Furthermore, our results also prove that layered-division multiplexing can cope better with receiver mobility than traditional time-division multiplexing when multiple services are intended in the same radio frequency channel.

KEYWORDS
Coverage probability, mobile broadcasting, multi-antenna diversity, receiver-on-vehicle

1 | INTRODUCTION

Motivated by the recent advances in self-driving technologies, infrastructure-to-vehicle (X2V) data delivery has attracted significant attention from both industry and academia. The contribution of the Media and Entertainment (M&E) vertical has appeared especially notable because a progressive evolution in driving-time activities is expected in the near future [1–3]. According to increasing demand for high-quality content and immersive meta-services, mobile broadcasting has been rediscovered to be a key momentum for such *multimedia-in-vehicle* movement, owing to the excellent point-to-multipoint (PTM) efficiency of terrestrial broadcasting [4–10]. The role of mobile broadcasting in the upcoming autonomous era has been identified as key for intelligent traffic systems as well, because automobile intelligence requires a legion of vehicles to acquire common, highly enhanced map data and accurate traffic information at the same time.

However, providing high-quality multimedia to mobile users through forward-link-only networks has been a complicated task for wireless systems [11,12]. Although the waveform of terrestrial broadcasting used to be more robust than that of high-capacity-mode cellular unicasts [13–16], mobile reliability in terrestrial broadcast systems is challenging because the broadcast lacks return channel feedback. The downlink-only nature of broadcasting enables arbitrary PTM transmissions

with reduced overhead and ensures static data traffic [17,18]. However, broadcasting loses the ability to adapt waveform/resources, which plays a powerful role in coping with dynamic channel gain fluctuations and mobility-entailed interference such as inter-carrier interference (ICI) [11,19]. The lessons from the previous, yet immature, efforts at mobile broadcast have revealed that a seamless and reliable service for moving users requires excessively dense gap-filler deployment [20–22].

In effect, for on-vehicle users, it is possible to exploit multi-antenna diversity to alleviate undesirable fading effects and further improve channel quality [11]. Since terrestrial broadcasting typically utilizes very-high frequency (VHF) and ultra-high frequency (UHF) bands that come with wavelengths 10^{-1} m to 10^{0} m in scale, it is difficult to deploy multiple antennas on handheld receivers (Rxs). In contrast, installing multiple antennas on mass-transportation vehicles, which are generally spacious, is a feasible idea for distributing mobile multimedia to the public.

In this paper, the multi-antenna diversity gain in mobile environments is therefore analyzed in terms of coverage probability. Based on analytical derivations, the diversity gain is verified with respect to Rx velocity, ergodic field strength, and threshold-of-visibility (ToV). The advantages of multi-antenna receivers (MRs) are investigated with respect to various aspects, including the geometric coverage, volume of the users served, and impact of Rx velocity. Furthermore, the feasibility of an MR in the real world is examined by extensive field experiments based on on-air ATSC 3.0 broadcast transmissions, accomplished by a full-chain ATSC 3.0 facility in Jeju Island, Republic of Korea. Relying on the erroneous second ratio (ESR) criterion, our practical evaluations demonstrate that MRs with a few more antennas achieve substantial reliability gains over single-antenna Rxs (SRs). The field test results reveal the possibility of mobile full-high-definition/ultra-high-definition (FHD/UHD) over terrestrial broadcasts, which can be achieved without deploying excessively dense gap-fillers or transmitters (Txs).

The remainder of this paper is organized as follows. Section 2 describes the system model for MRs in a mobile environment. Section 3 analytically derives the coverage probability gains of MRs over SRs based on the model described in Section 2. The results in Section 3 are extended to demonstrate the benefits of layered division multiplexing (LDM) for mobile services in Section 4. Numerical results and field experiment results are presented and discussed in Sections 5 and 6, respectively, thereby verifying MR gains from analytical and empirical perspectives, respectively. Finally, Section 7 concludes the paper with some remarks.

2 | SYSTEM MODEL

This paper considers a single-input multiple-output (SIMO) network with an Rx performing maximal ratio combining (MRC) through N antennas. The Rx is assumed to travel at a speed v and is usually assumed to be installed on a vehicle. We here refer to typical orthogonal frequency-division multiplexing (OFDM) transmission for signal modeling, but do not address the detailed system architecture until Section 6. Therefore, because of the mobility of the Rx, the received signal suffers from ICI, whose variance is proportional to the power of the desired signal.

Precisely, the signal-to-interference-plus-noise ratio (SINR) of the received signal is calculated as

$$\gamma_{\text{div}} = \frac{\sum_{i=1}^{N} |h_i|^2 P_{\text{R}}}{1 + c_{\text{ICI}} \sum_{i=1}^{N} |h_i|^2 P_{\text{R}}}, \tag{1}$$

where c_{ICI} denotes the relative variance level of the ICI compared to the desired signal power. Referring to various studies related to ICI effects within OFDM, for example, [19], c_{ICI} can be approximated as $c_{\text{ICI}} \approx 1/24(2\pi f_c v/cT_s)^2$ for Jakes' scattering environment, where c represents the speed of light, and f_c and T_s denote the center frequency and symbol duration, respectively. The Rayleigh channel is assumed for small-scale fading. That is, the small-scale fading gains $h_{i=1,\cdots,N} \in \mathbb{C}$ in (1), where h_i corresponds to the i th antenna of the Rx, are defined to be independent and identically distributed (IID) complex Gaussian random variables with zero mean and unit variance. In addition, $P\text{R} \in \mathbb{R}^+$ denotes the ergodic average power normalized by the thermal noise variance, at which large-scale fading is reflected with respect to the Rx location.

Our goal is to observe the gain of MR over SR under a given P_{R}. To observe this gain, we specify a $N = 1$ case by defining the SINR of single-antenna reception as $\gamma_s = \frac{|h_s|^2 P_{\text{R}}}{1 + c_{\text{ICI}}|h_s|^2 P_{\text{R}}}$. As for γ_s, the small-scale fading gain h_s: $\mathscr{CN}(0,1)$ is additionally defined for the SR channel to distinguish it from h_i s.

3 | COVERAGE PROBABILITY GAIN FROM DIVERSITY RECEIVING

Since this work addresses a broadcast scenario, the desired data are transmitted at a fixed rate. Accordingly, the Tx is allowed to transmit broadcast signals with a service rate of $\text{R}_a = B\log_2(1+\varepsilon_{\text{th}})$ [bps] for $^{\exists}B > 0$ [Hz] bandwidth and $^{\exists}\varepsilon_{\text{th}} > 0$. This means that an Rx requires an SINR of at least ε_{th} to retrieve the original message. Therefore, for locations at which the Rx acquires an average signal power P_{R} (a P_{R}-*region* $\Phi(P_{\text{R}})$, in short), the coverage probability at the MR is given as follows:

$$\begin{aligned} P_{\text{div}} &\triangleq \Pr[\gamma_{\text{div}} \geq \varepsilon_{\text{th}}] = \Pr\left[\sum_{i=1}^{N} |h_i|^2 \geq \frac{\varepsilon_{\text{th}}}{(1 - c_{\text{ICI}}\varepsilon_{\text{th}})P_{\text{R}}}\right] \\ &\overset{(a)}{=} \frac{1}{\Gamma(N)}\Gamma\left(N, \frac{\varepsilon_{\text{th}}}{(1 - c_{\text{ICI}}\varepsilon_{\text{th}})P_{\text{R}}}\right), \end{aligned} \tag{2}$$

where (a) holds since $\sum_{i=1}^{N} |h_i|^2$ follows a chi-squared distribution whose cumulative density function (CDF) is $1-\Gamma(N,z)/\Gamma(N)$; $\Gamma(s)=\int_0^\infty t^{s-1}\exp(-t)dt$ and $\Gamma(s,z)=\int_z^\infty t^{s-1}p(-t)dt$ denote the gamma function and upper incomplete gamma function, respectively. Owing to the alternative expressions of the gamma functions, (2) are rewritten as

$$P_{\text{div}} = \exp\left(-\frac{\varepsilon_{\text{th}}}{\left(1-c_{\text{ICI}}\varepsilon_{\text{th}}\right)P_{\text{R}}}\right)\sum_{k=0}^{N-1}\frac{1}{k!}\left(\frac{\varepsilon_{\text{th}}}{\left(1-c_{\text{ICI}}\varepsilon_{\text{th}}\right)P_{\text{R}}}\right)^{k}, \quad (3)$$

which is a better and more tractable form than (2). As a corollary, the counterpart for SR is given in a reduced form as

$$P_s \triangleq \Pr\left[\gamma_s \geq \varepsilon_{\text{th}}\right] = \exp\left(-\frac{\varepsilon_{\text{th}}}{\left(1-c_{\text{ICI}}\varepsilon_{\text{th}}\right)P_{\text{R}}}\right). \quad (4)$$

A coverage probability is in essence a complementary CDF of the aggregate small-scale fading gain. Statistically, the main factor that brings an MR gain is the fact that a chi-squared distribution with a higher distribution order becomes less concentrated in low-value realizations. The increase in MRC branches shifts the weights within the distribution toward high-value realizations and eventually brings the following asymptote.

Remark 1 (The coverage probability at an MR asymptotically approaches 1 as N increases): Note that the polynomial term in (3) is the first N parts of the Taylor expansion of $\exp\left(\varepsilon_{\text{th}}/\left(1-c_{\text{ICI}}\varepsilon_{\text{th}}\right)/P_{\text{R}}\right)$. Accordingly, it can be found that the polynomial term of (3) finally approaches $\exp\left(\varepsilon_{\text{th}}/\left(1-c_{\text{ICI}}\varepsilon_{\text{th}}\right)/P_{\text{R}}\right)$ as $N\to\infty$. This observation indicates that an MR with an infinite number of antennas always succeeds at decoding, so it supports the utility of a massive antenna installation at the on-vehicle Rxs.

Based on previous formulations, the gain of MR over SR can be measured in two distinct forms: a relative gain and an absolute gain. The relative gain quantifies the MR gain by a ratio between the coverage probabilities of MR and SR, whereas the absolute gain deals with the difference in the coverage probability between MR and SR. Namely, the relative and absolute gains are defined as

$$\Delta^{\text{rel}} \triangleq \frac{P_{\text{div}}}{P_{\text{s}}} = \sum_{k=0}^{N-1}\frac{1}{k!}\left(\frac{\varepsilon_{\text{th}}}{\left(1-c_{\text{ICI}}\varepsilon_{\text{th}}\right)P_{\text{R}}}\right)^{k}, \quad (5)$$

and

$$\Delta^{\text{abs}} \triangleq P_{\text{div}} - P_{\text{s}} = \exp\left(-\frac{\varepsilon_{\text{th}}}{\left(1-c_{\text{ICI}}\varepsilon_{\text{th}}\right)P_{\text{R}}}\right)\sum_{k=1}^{N-1}\frac{1}{k!}\left(\frac{\varepsilon_{\text{th}}}{\left(1-c_{\text{ICI}}\varepsilon_{\text{th}}\right)P_{\text{R.}}}\right)^{k}, \quad (6)$$

respectively. One can see that Δ^{rel}, whose polynomial coefficients are strictly positive, monotonically increases by $\varepsilon_{\text{th}}/\left(1-c_{\text{ICI}}\varepsilon_{\text{th}}\right)/P_{\text{R}}$, whereas Δ^{abs} can be a multimodal function of $\varepsilon_{\text{th}}/\left(1-c_{\text{ICI}}\varepsilon_{\text{th}}\right)/P_{\text{R}}$ owing to its exponential term. In addition, one can draw the following results from expressions (5) and (3).

Observation 1: If $N\geq 2$, Δ^{rel} strictly increases by $\varepsilon_{\text{th}}/\left(1-c_{\text{ICI}}\varepsilon_{\text{th}}\right)/P_{\text{R}}$.

Let x abbreviate $\varepsilon_{\text{th}}/\left(1-c_{\text{ICI}}\varepsilon_{\text{th}}\right)/P_{\text{R}}$. The derivative of $\sum_{k=0}^{N-1}x^k/k!$ with respect to x is strictly positive for $^{\forall}x>0$. Therefore, $\Delta^{\text{rel}}(x)$ strictly increases by x. ∎

Remark 2 (Advantages for high-throughput services): The interests of network operators and service providers may be particularly focused on the relationship between Δ^{rel} and R_a. We note that $\varepsilon_{\text{th}}/\left(1-c_{\text{ICI}}\varepsilon_{\text{th}}\right)/P_{\text{R}}$ increases by ε_{th}, and hence one can find from (5) that Δ^{rel} increases by ε_{th} $(=2^{R_{a/B}}-1)$. This implies that MR is more beneficial for high-throughput services, from a relative gain perspective. Moreover, because $\Delta^{\text{rel}}|_{N+1}-\Delta^{\text{rel}}|_{N}=\left(\varepsilon_{\text{th}}/\left(1-c_{\text{ICI}}\varepsilon_{\text{th}}\right)/P_{\text{R}}\right)^{N+1}/(N+1)!$ holds, the advantage of adding a single additional antenna appears greater when ε_{th} increases.

Observation 2: If $N\geq 2$, Δ^{rel} strictly decreases by P_{R}.

Let x abbreviate $\varepsilon_{\text{th}}/\left(1-c_{\text{ICI}}\varepsilon_{\text{th}}\right)/P_{\text{R}}$ again. The derivative of $\sum_{k=0}^{N-1}x^k/k!$ with respect to P_{R}

$$\frac{\partial x}{\partial P_{\text{R}}}\frac{\partial}{\partial x}\left(\sum_{k=0}^{N-1}\frac{1}{k!}x^k\right) = -\frac{\varepsilon_{\text{th}}}{\left(1-c_{\text{ICI}}\varepsilon_{\text{th}}\right)P_{\text{R}}^2}\frac{\partial}{\partial x}\left(\sum_{k=0}^{N-1}\frac{1}{k!}x^k\right),$$

is then found to be strictly negative for $^{\forall}P_{\text{R}}>0$ and $^{\forall}x>0$ owing to Observation 1. ∎

Observation 3: If $N\geq 2$, Δ^{abs} is maximized at

$$P_{\text{R}}^{*} \triangleq \frac{\varepsilon_{\text{th}}}{\left(1-c_{\text{ICI}}\varepsilon_{\text{th}}\right)\sqrt[N-1]{(N-1)!}}. \quad (7)$$

By using the abbreviation $x\triangleq\varepsilon_{\text{th}}/(1-c_{\text{ICI}}\varepsilon_{\text{th}})/P_{\text{R}}$, the derivative of Δ^{abs} can be obtained as

$$\frac{\partial\Delta^{\text{abs}}}{\partial x} = \left(1-\frac{x^{N-1}}{(N-1)!}\right)\exp(-x),$$

where $\partial\Delta^{\text{abs}}/\partial x=0$ holds at $x=\sqrt[N-1]{(N-1)!}$. Because $\Delta^{\text{abs}}(x=0)=0$ is strictly smaller than $\Delta^{\text{abs}}\left(x=\sqrt[N-1]{(N-1)!}\right)$ and the derivative $\partial\Delta^{\text{abs}}/\partial x$ for $x>0$ is positive only until $x\geq\sqrt[N-1]{(N-1)!}$, this local maximum is the global maximum point of Δ^{abs}. ∎

In the case in which the MR is equipped with two antennas, it is able to specify the ε_{th} and P_{R} values that allow the MR to achieve the target absolute gain Δ_{TG} over an SR, that

is, $\arg_{(\varepsilon_{\text{th}},P_{\text{R}})}\left(\Delta^{\text{abs}}=\Delta_{\text{TG}}\right)$. For $N=2$, the absolute gain of an MR over an SR is given by

$$\Delta^{\text{abs}}|_{N=2}=\frac{\varepsilon_{\text{th}}}{\left(1-c_{\text{ICI}}\varepsilon_{\text{th}}\right)P_{\text{R}}}\exp\left(-\frac{\varepsilon_{\text{th}}}{\left(1-c_{\text{ICI}}\varepsilon_{\text{th}}\right)P_{\text{R}}}\right). \quad (8)$$

Accordingly, the pair of ε_{th} and P_{R} should satisfy

$$\frac{\varepsilon_{\text{th}}}{\left(1-c_{\text{ICI}}\varepsilon_{\text{th}}\right)P_{\text{R}}}=-W_{-1}\left(-\Delta_{\text{TG}}\right)\overset{(b)}{\approx}\frac{1}{4}+\sqrt{2\ln\left(\frac{1}{\Delta_{\text{TG}}}\right)-2}+\frac{3}{4}\ln\left(\frac{1}{\Delta_{\text{TG}}}\right). \quad (9)$$

to achieve the Δ^{abs} of Δ_{TG}, where $W_{-1}(\cdot)$ denotes the lower branch of the Lambert W function. Approximation (b) in (9) is due to the result in [23]. Additionally, it should be noted that Δ_{TG} can take a value only in $\left[0,1/e\right]$ because $1/e$ is the maximum value of Δ^{abs}.

Remark 3 (Effectiveness of MR in low-P_{R} fields): The context in Observation 3 encourages the use of MR in low-P_{R} locations. Note that $\max\left(\Delta^{\text{abs}}\right)$ and P_{R}^{*} are monotonically increasing and decreasing functions for N, respectively, which allows us to argue for the benefits of MR at low-P_{R} locations. As shown in Figure 1, the MR gain at $\max\left(\Delta^{\text{abs}}\right)$ is especially notable for small N s. In other words, additional installation of a few more antennas provides substantial P_{div} gain at P_{R}^{*}, which is supposed to be low. Recalling Figure 1, using four antennas yields a $\max\left(\Delta^{\text{abs}}\right)$ of 70% and increasing the number of antennas to seven increases $\max\left(\Delta^{\text{abs}}\right)$ beyond 90%.

Remark 4 (Connection with network field testing): In practice, statistics based on empirical measurements are typically used for evaluating mobile network deployments. For example, ITU-R recommends evaluating networks using the ESR criterion when the field measurements are conducted by driving through a network coverage area [24]. The field test reports following the ITU-R recommendation usually analyze ESR curves with respect to field strength to determine how many reception successes (or failures) are observed under each (average) field strength [25]. This approach lies in the same vein as the coverage probability concept discussed in this paper, so we emphasize that coverage probability could play a role as a theoretical counterpart to the ESR measure.

Remark 5 (Geometric coverage perspective): The results in Observations 1–3 can also provide an intuition for geometric service coverage as well as the number of service-available users. If we assume that a population of potential users is uniform over a two-dimensional geometric field, then a convincing propagation loss model connects P_{div} to valuable insights for determining the geometric/demographic coverage.

Let the propagation loss be defined as $F(r)\triangleq\frac{P_{\text{R}}(r)}{P_{\text{T}}}$, where the transmission power, measured at the reference distance $r_0>0$ is

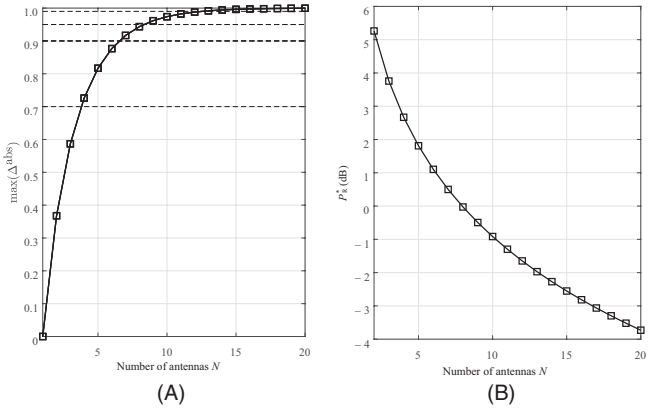

FIGURE 1 MR gain $\max\left(\Delta_{\text{abs}}\right)$ vs. N

denoted as $P_{\text{T}}\geq 0$ and $r\geq r_0$ denotes the distance between the Rx and Tx. The expression $P_{\text{R}}(r)$ is here used to note the dependency of P_{R} on r. As is generally known, $F(r)$ is expected to be a monotonically decreasing function of r. Therefore, when at least $^{\exists}p_{\text{TG}}\geq 0$ coverage probability is desired for the network, the maximum r that allows $P_{\text{div}}\geq p_{\text{TG}}$ can be expressed as

$$r_{\text{edge}}\left(N,\varepsilon_{\text{th}},P_{\text{R}}^{\text{TG}}\right)\triangleq F^{-1}\left(\frac{P_{\text{R}}^{\text{TG}}}{P_{\text{T}}}\right). \quad (10)$$

for $P_{\text{R}}^{\text{TG}}\triangleq P_{x}^{-1}(p_{\text{TG}})$ with $\chi\in\{div,s\}$. Simply speaking, r_{edge} refers to the distance to the coverage edge, in which the target coverage probability p_{TG} is to be guaranteed at the coverage edge. Note that r_{edge} is definitely dependent on N and ε_{th}. As we assume the transmission and propagation are isotropic, the network's geometric coverage $\mathscr{A}_N$ is expected to be a disk with a size of

$$\left|\mathscr{A}_N\right|=\pi r_{\text{edge}}^{2}. \quad (11)$$

for an N-antenna MR ($N=1$ is for an SR). This representation allows us to calculate the coverage area gain of an MR by

$$\frac{\left|\mathscr{A}_N\right|}{\left|\mathscr{A}_1\right|}=\left(\frac{r_{\text{edge}}\left(N,\varepsilon_{\text{th}},P_{\text{div}}^{-1}\left(p_{\text{TG}}\right)\right)}{r_{\text{edge}}\left(1,\varepsilon_{\text{th}},P_{\text{s}}^{-1}\left(p_{\text{TG}}\right)\right)}\right)^{2}, \quad (12)$$

which is also equal to the ratio of the amount of service-available users if the user distribution is given as uniform.

Remark 6 (Channel correlation effect): In practice, an MR might suffer from unexpected degradation due to the correlation among channel branches. The report in [26] showed that a multi-antenna channel can be correlated even when the spacing between all adjacent antennas exceeds $\lambda/2$, especially under far-field conditions. By referring to [26] and [27], the modified small-scale fading channel can be expressed as $\tilde{\mathbf{h}}\triangleq\mathbf{h}\mathbf{R}^{1/2}$, where $\mathbf{h}\triangleq\left[h_1,h_2,\cdots,h_N\right]$ comprehensively represents the Rayleigh fading components in vector form and $\mathbf{R}$

represents the channel correlations among the receive antennas. A $\lambda/2$-spaced uniform circular array correlation matrix $\mathbf{R}$ in a one-ring scattering model can be defined as

$$R_{m,\, n \in \{1,\, \ldots,\, N\}} = \frac{1}{2\eta} \int_{\theta-\eta}^{\theta+\eta} \exp(j\pi(m-n)\sin\phi) d\phi, \quad (13)$$

where θ is the relative angle of arrival and η is the angular spread [26]. Let $\{\sigma_i^2\}_{i \in \{1,\, \ldots,\, N\}}$ denote the eigenvalues of $\mathbf{R}$. Since the elements of $\mathbf{h}$ follow IID $\mathcal{CN}(0,1)$, $||\tilde{\mathbf{h}}||^2$ conforms to a generalized chi-squared distribution with coefficients σ_i^2 s, whose PDF is given as $f_{\text{corr}}(x) = \sum_{i}^{N} \frac{\exp\left(-\frac{x}{\sigma_i^2}\right)}{\sigma_i^2 \prod_{\substack{j=1 \\ j \neq i}}^{N} \left(1 - \frac{\sigma_j^2}{\sigma_i^2}\right)}$ when every σ_i is different from the others.

Such rearrangement induces a certain degradation of P_{div}. Figure 2 presents an example of this degradation by comparing the PDFs of $||\mathbf{h}||^2$ and $||\mathbf{h}||^2$. For the correlated case, a 4-antenna $\mathbf{R}$ with $\theta = \pi/4$ and $\eta = 2\pi$ is considered, which has $[\sigma_1^2, \sigma_2^2, \sigma_3^2, \sigma_4^2\,[=]\,1.3042, 1.1812, 0.7349, 0.7797]$. As shown in Figure 2, $||\tilde{\mathbf{h}}||^2$ is more concentrated at the lower realizations than $||\mathbf{h}||^2$, so P_{div} is decreased as a consequence. Note that our previous results on P_{div} drawn from the non-correlated case can easily be revised by taking $||\tilde{\mathbf{h}}||^2$ into account, since $f_{\text{corr}}(x)$ is given in a tractable exponential form.

Remark 7 (SIMO-MISO duality): Similar to many studies that have tackled the equivalence of SIMO and multiple-input single-output (MISO), our approach can be readily applied to MISO systems in single frequency networks (SFNs) [28–30]. Note that on the one hand, [11] has verified the SFN diversity to enhance the signal robustness against channel mobility via extensive simulations. If we consider an SFN with N Txs, each MR channel branch can be mapped to the Tx-to-Rx channels of the MISO dual system. However, the overall MRC-combined channel gain in the MISO case would be realized by a generalized chi-squared distribution, that is, to follow $f_{\text{corr}}(\cdot)$, because the Rx distances from each Tx will probably be different from each other, unlike in the SIMO case. Moreover, the MRC could not always be properly obtained in MISO SFNs since the delay control of SFN could not be appropriate for every reception at an arbitrary location. On the contrary, SIMO also has a potential drawback in that MR channel branches are more likely to be correlated in practice.

4 | LDM GAIN FOR MOBILE RECEPTION

In addition to the MR gain, the spectrally efficient feature of LDM can further help handling the difficulties in mobile environments. In this section, we reveal that LDM tolerates ICI better than TDM. Here, the standard *two-layer* LDM of the ATSC 3.0 is addressed. The receptions of two different transmission layers of LDM, that is, the core layer (CL) and enhanced layer (EL), are separately addressed in Sections 4.1 and 4.2, respectively. To guarantee fairness, the comparisons presented below are drawn under the *identical stationary user coverage* assumption, which means that the LDM and TDM services of interest are constrained to have equivalent service coverage for non-mobile users.

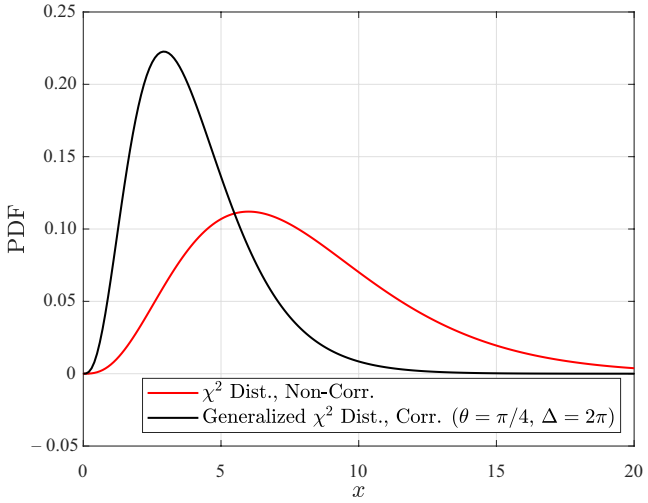

FIGURE 2 Probability density functions (PDFs) of aggregate channel gains with and without channel correlations ($N = 4$, $\theta = \pi/4$, and $\eta = 2\pi$ for the channel-correlated case)

4.1 | Mobile reception of LDM CL

We first address the case in which the desired signal is conveyed by the LDM CL, whereas the EL, whose power is $\delta \in (0,1)$ times lower than that of the CL, is regarded as additive inter-layer interference (ILI) to the desired signal [31–34]. To match coverage areas between the LDM CL and TDM to be the same for their stationary (that is, non-mobile) services, the following shall be satisfied:

$$\frac{1}{\varepsilon_{\text{LDM}}^{\text{CL}}} = \delta + \frac{1+\delta}{\varepsilon_{\text{TDM}}^{\text{CL}}}, \quad (14)$$

where $\varepsilon_{\text{LDM}}^{\text{CL}}$ and $\varepsilon_{\text{TDM}}^{\text{CL}}$ denote the ToVs of the LDM CL and TDM transmissions, respectively, specifically for the case in which CL conveys the desired signal in the LDM transmissions.

Using the general expression for MR, one can find the SINR of LDM CL signal to be $\gamma_{\text{div, LDM}}^{\text{CL}} = \frac{\sum_{i=1}^{N} |h_i|^2 \frac{P_{\text{R}}}{1+\delta}}{1 + \sum_{i=1}^{N} |h_i|^2 \frac{\delta P_{\text{R}}}{1+\delta} + c_{\text{ICI}} \sum_{i=1}^{N} |h_i|^2 \frac{P_{\text{R}}}{1+\delta}}$, which involves ILI and ICI in the denominator term. A coverage probability of an LDM CL is then defined as

$$P_{\mathrm{LDM}}^{\mathrm{CL}}=\Pr\left[\frac{\sum_{i=1}^{N}|h_i|^2\frac{P_{\mathrm{R}}}{1+\delta}}{1+\sum_{i=1}^{N}|h_i|^2\frac{\delta P_{\mathrm{R}}}{1+\delta}+c_{\mathrm{ICI}}\sum_{i=1}^{N}|h_i|^2\frac{P_{\mathrm{R}}}{1+\delta}}\geq\varepsilon_{\mathrm{LDM}}^{\mathrm{CL}}\right]$$

$$=\Pr\left[\sum_{i=1}^{N}|h_i|^2\geq\frac{(1+\delta)\,\varepsilon_{\mathrm{LDM}}^{\mathrm{CL}}}{\left(1-\delta\varepsilon_{\mathrm{LDM}}^{\mathrm{CL}}-c_{\mathrm{ICI}}\varepsilon_{\mathrm{LDM}}^{\mathrm{CL}}\right)P_{\mathrm{R}}}\right]. \tag{15}$$

under a given average field strength P_{R}. Likewise, the counterpart for the TDM case is given as

$$P_{\mathrm{LDM}}^{\mathrm{CL}}=\Pr\left[\sum_{i=1}^{N}|h_i|^2\geq\frac{\varepsilon_{\mathrm{TDM}}^{\mathrm{CL}}}{\left(1-c_{\mathrm{ICI}}\varepsilon_{\mathrm{TDM}}^{\mathrm{CL}}\right)P_{\mathrm{R}}}\right]. \tag{16}$$

Note that the comparison between $P_{\mathrm{LDM}}^{\mathrm{CL}}$ and $P_{\mathrm{TDM}}^{\mathrm{CL}}$ is determined by the superiority/inferiority between $\varepsilon_{\mathrm{TDM}}^{\mathrm{CL}}/\left(1-c_{\mathrm{ICI}}\varepsilon_{\mathrm{TDM}}^{\mathrm{CL}}\right)$ and $(1+\delta)\,\varepsilon_{\mathrm{LDM}}^{\mathrm{CL}}/\left(1-\delta\varepsilon_{\mathrm{TDM}}^{\mathrm{CL}}-c_{\mathrm{ICI}}\varepsilon_{\mathrm{TDM}}^{\mathrm{CL}}\right)$. From (14), the equivalence

$$\frac{(1+\delta)\,\varepsilon_{\mathrm{LDM}}^{\mathrm{CL}}}{1-\delta\varepsilon_{\mathrm{LDM}}^{\mathrm{CL}}-c_{\mathrm{ICI}}\varepsilon_{\mathrm{LDM}}^{\mathrm{CL}}}<\frac{\varepsilon_{\mathrm{TDM}}^{\mathrm{CL}}}{1-c_{\mathrm{ICI}}\varepsilon_{\mathrm{LDM}}^{\mathrm{CL}}}\Leftrightarrow\frac{1}{\varepsilon_{\mathrm{LDM}}^{\mathrm{CL}}}-c_{\mathrm{ICI}}\delta<\frac{1}{\varepsilon_{\mathrm{LDM}}^{\mathrm{CL}}}. \tag{17}$$

can be obtained, where the right-hand side is valid for $^{\forall}c_{\mathrm{ICI}}\delta>0$. Consequently, $P_{\mathrm{LDM}}^{\mathrm{CL}}>P_{\mathrm{TDM}}^{\mathrm{CL}}$ is obtained, which implies that LDM is preferable for mobile services.

4.2 | Mobile reception of LDM EL

LDM transmissions would be beneficial not just for the CL-desired case, but also for the case when EL conveys the desired service. When the EL is allowed to be transmitted with power that is δ times lower than that of the CL, as in Section 4.1, matching the coverage between LDM EL and TDM for stationary service gives.

$$\varepsilon_{\mathrm{LDM}}^{\mathrm{EL}}=\frac{1+\delta}{\delta}\varepsilon_{\mathrm{TDM}}^{\mathrm{EL}}. \tag{18}$$

similarly to (14), where $\varepsilon_{\mathrm{LDM}}^{\mathrm{EL}}$ and $\varepsilon_{\mathrm{TDM}}^{\mathrm{EL}}$ denote the ToV of LDM EL and TDM transmission for the EL-desired case, respectively. Unlike in CL, ILI is removed by successive interference cancellation before decoding EL signals, and hence the effective SINR of EL can be found to be $\gamma_{\mathrm{div,\,LDM}}^{\mathrm{EL}}=\frac{\sum_{i=1}^{N}|h_i|^2\frac{\delta P_{\mathrm{R}}}{1+\delta}}{1+c_{\mathrm{ICI}}\sum_{i=1}^{N}|h_i|^2P_{\mathrm{R}}}$ (see [4] and therein). In fact, we note that the CL component in ICI is not removed from the received signal, which causes the Rx to suffer from $c_{\mathrm{ICI}}\sum_{i=1}^{N}|h_i|^2P_{\mathrm{R}}$ of the ICI power during EL decoding. In consequence, the coverage probabilities of LDM EL and TDM can be expressed as

$$P_{\mathrm{LDM}}^{\mathrm{EL}}=\Pr\left[\sum_{i=1}^{N}|h_i|^2\geq\frac{\frac{1+\delta}{\delta}\varepsilon_{\mathrm{LDM}}^{\mathrm{EL}}}{\left(1-\frac{1+\delta}{\delta}c_{\mathrm{ICI}}\varepsilon_{\mathrm{LDM}}^{\mathrm{EL}}\right)P_{\mathrm{R}}}\right]$$

$$=\Pr\left[\sum_{i=1}^{N}|h_i|^2\geq\frac{\varepsilon_{\mathrm{TDM}}^{\mathrm{EL}}}{\left(1-c_{\mathrm{ICI}}\varepsilon_{\mathrm{TDM}}^{\mathrm{EL}}\right)P_{\mathrm{R}}}\right]. \tag{19}$$

and

$$P_{\mathrm{TDM}}^{\mathrm{EL}}=\Pr\left[\sum_{i=1}^{N}|h_i|^2\geq\frac{\varepsilon_{\mathrm{TDM}}^{\mathrm{EL}}}{\left(1-c_{\mathrm{ICI}}\varepsilon_{\mathrm{TDM}}^{\mathrm{EL}}\right)P_{\mathrm{R}}}\right], \tag{20}$$

respectively, for a given P_{R}. Equations 19 and (20) clearly show that $P_{\mathrm{LDM}}^{\mathrm{EL}}=P_{\mathrm{TDM}}^{\mathrm{EL}}$. This result may imply that LDM and TDM are theoretically equivalent for mobile reception when EL is desired at the Rx.

However, it should be noted that (18) deals with the situation in which LDM EL is forced to have the same stationary service coverage with TDM. In addition, the previous studies have thoroughly verified that LDM provides significantly better spectral efficiency than TDM when multiple services with unequal error protections are intended. Moreover, LDM in practice may even offer more efficient framing with less overhead.[1] If (18) is satisfied, LDM EL would probably be able to send substantially more data than the TDM configuration. In other words, LDM could probably use the reserved spectral ability to expand the coverage (that is, lowering $\varepsilon_{\mathrm{LDM}}^{\mathrm{EL}}$ from that of (18)). Regarding the previous equalities of (19) and (20), $P_{\mathrm{LDM}}^{\mathrm{EL}}$ may become higher than $P_{\mathrm{TDM}}^{\mathrm{EL}}$ because of the decreased $\varepsilon_{\mathrm{LDM}}^{\mathrm{EL}}$. Thus, LDM transmissions would be preferable to TDM even when the EL contains the desired service.

5 | NUMERICAL RESULTS

The coverage gain of MR was numerically verified before the empirical field trials in a real environment. The simulations were obtained for a $f_c=600$ MHz carrier frequency to analyze the MR effect in the UHF band, which is typical for terrestrial broadcasting in various countries. Referring to the ATSC 3.0 physical layer specification A/322 [35], the transmit signals were considered to have $\mathrm{T}_s=1/419$ s, assuming an ATSC 3.0 waveform with a $\mathrm{B}=6$ MHz bandwidth and 16K-sized FFT. Accounting for mobile services in particular, the coverage probability gain was analyzed for a service with $\varepsilon_{\mathrm{th}}=5$ dB ToV, which ensures a $\mathrm{Blog}_2\left(1+\varepsilon_{\mathrm{th}}\right)=12.3442$ Mbps throughput capacity.

[1]The use of LDM in ATSC 3.0 reduces the signaling information defining the time interleaving for the physical layer pipes (PLPs) mapped into EL. Moreover, LDM may offer an additional overhead-reduction gain for other subframe parameters, particularly when the counterpart TDM example requires multiple subframes (see [35]).

In Figure 3A, the absolute gain Δ^{abs} of MR over SR is presented with respect to P_{R}. The MR scenarios with $N = 2, 3, 4, 10$ were addressed specifically for the MR vs. SR comparison. As shown in the plots above, the maximum peak of Δ^{abs}, denoted by $\max\left(\Delta^{\text{abs}}\right)$, increased by N, and the peaks arose at the lower P_{R}^{*} s as N increased. Note that P_{R}^{*} is a monotonically decreasing function of N. Figure 3B accordingly reveals that an MR with larger N provides a significant improvement in coverage, especially in low-P_{R} regions. In addition, Figure 3B validates the argument of Remark 2. An MR was demonstrated to be more beneficial for high-throughput services, and this advantage was more apparent for faster Rxs because the effective ToV $\varepsilon_{\text{th}}/\left(1-c_{\text{ICI}}\varepsilon_{\text{th}}\right)$ in Figure 3C increased more rapidly for higher values of v.

Figure 4 shows P_{div} and P_s over the reception signal strengths for the case the Rx goes through -90 dBm of system noise. Clearly shown by the inflection point shifts, MR substantially enhanced the coverage probability as N increased. Recalling Remark 1, the MR will attain $P_{\text{div}} = 1$ for every P_{R} as N approaches infinity. In the simulations, the MR with $N = 4$ required a signal strength 8 dB less than that required by SR to guarantee a 95 % coverage probability, where -72 dBm, -80 dBm, -86 dBm, and -92 dBm were required for 95 % reception for SR, $N = 2$, $N = 4$, and $N = 10$, respectively.

Remark 8 (Rx velocity effect): We also investigated the effect of the Rx velocity through the calculations plotted in Figure 5. As can be inferred from the proportional dependency of c_{ICI} to v^2, the reception failures drastically increased by v. For $P_{\text{R}} = -80$ dBm in particular, any of the Rxs with $N \leq 4$ were able to achieve a coverage probability of more than 10% at $v > 280$ km/h. However, an MR with more antennas was verified to offer a greater relative gain in harsh conditions, that is, a low-$P_{\chi\in\{\text{div},s\}}$ environment, with higher Rx velocity. As noted in Observation 1, installing additional antennas would be particularly advantageous in high-velocity Rxs.

In addition, Remark 5 was again analyzed through numerical calculations. In particular, an example of the well-known COST-231 Hata model was explored. According to the report [36], the path loss based on the urban Hata model is given by

$$\begin{aligned} 10\log_{10}\left(F\left(r\right)\right) = 46.3 + 33.9\log_{10} f_c - 13.82\log_{10} h_{\text{T}} \\ -a\left(h_{\text{R}}, f_c\right) + \left(44.9 - 6.55\log_{10} h_{\text{T}}\right)\log_{10} r + C_m. \end{aligned} \tag{21}$$

in a logarithm form with $a\left(h\text{R}, f_c\right) = 3.2(\log_{10}(11.75h\text{R}))^2 - 4.97$ and

$$C_m = \begin{cases} 0\text{dB}, \text{ medium cities, suburban areas} \\ 3\text{dB}, \text{ metropolitan areas} \end{cases}, \tag{22}$$

for $f_c \in 200, 1500]$ MHz, where $P_{\text{T}}, h_{\text{T}}, h_{\text{R}}$, and r denote the transmission power at the Tx, the heights of the Tx and Rx, and the distance between the Tx and Rx, respectively.

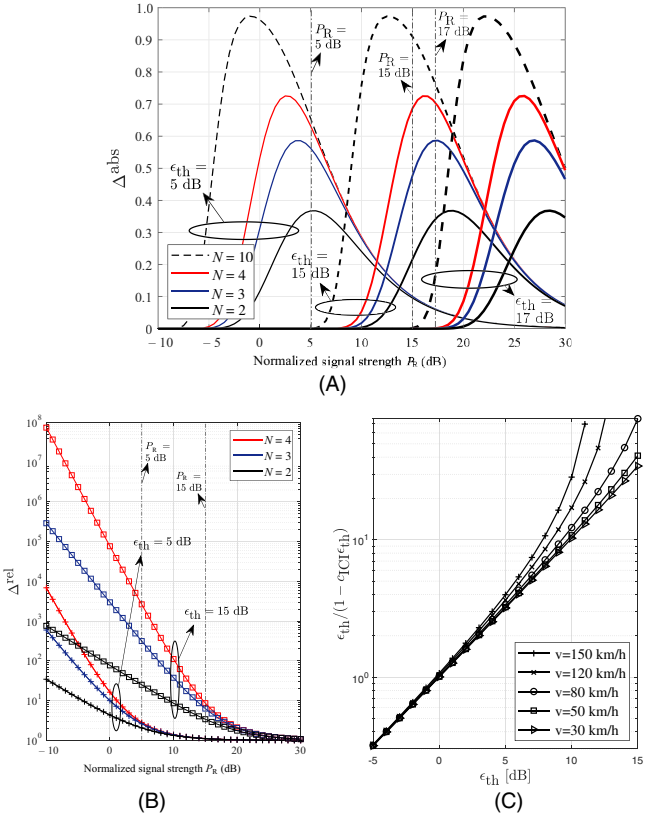

FIGURE 3 (A) Δ_{abs} vs. P_{R}, (B) Δ_{rel} vs. P_{R} ($\varepsilon_{\text{th}} = 5$ [dB], $v = 80$ [km/h], $f_c = 600$ [MHz], $\text{T}_s = 1/419$ [s]), and (C) $\varepsilon_{\text{th}}/\left(1 - c_{\text{ICI}}\varepsilon_{\text{th}}\right)$ vs. $\varepsilon_{\text{th}} f_c = 600$ [MHz], $T_s = 1/419$ [s])

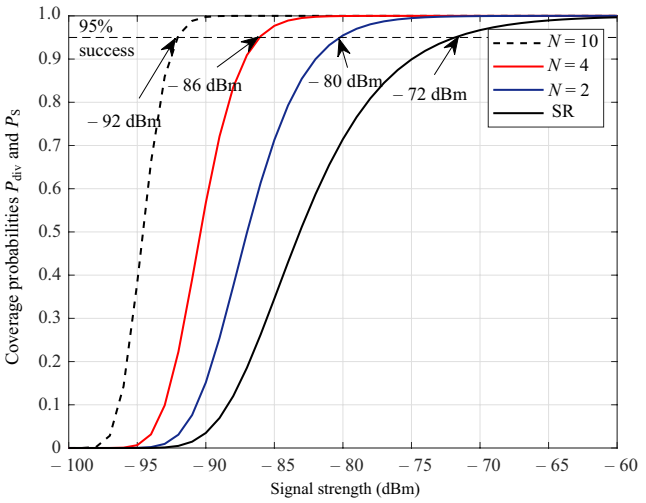

FIGURE 4 P_{div} and P_s vs. signal strength (noise level -90 [dBm], $\varepsilon_{\text{th}} = 5$ [dB], $v = 80$ [km/h], $f_c = 600$ [MHz], and $\text{T}_s = 1/419$ [s])

Based on (21), (3), and (4), the number of service-available users, whose distances from the Tx are in $\left[r_0, r\right]$, can be calculated from $n_N(r) \triangleq \int_{r_0}^{r} \left(P_{\chi\in\{div,s\}}(P_{\text{R}}(\zeta)\,|N) 2\pi\kappa\zeta d\zeta\right.$ by assuming the potential users to be uniformly distributed

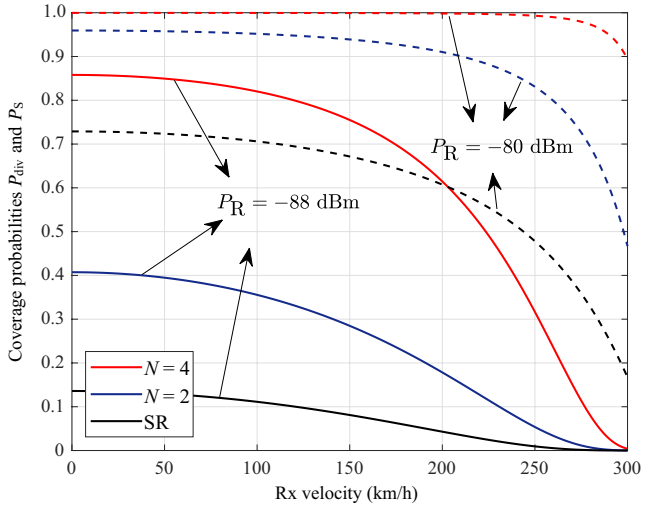

FIGURE 5 P_{div} and P_s vs. v (noise level −90 [dBm], $\epsilon_{th} = 5$ [dB], $f_c = 600$ [MHz], and $T_s = 1/419$ [s])

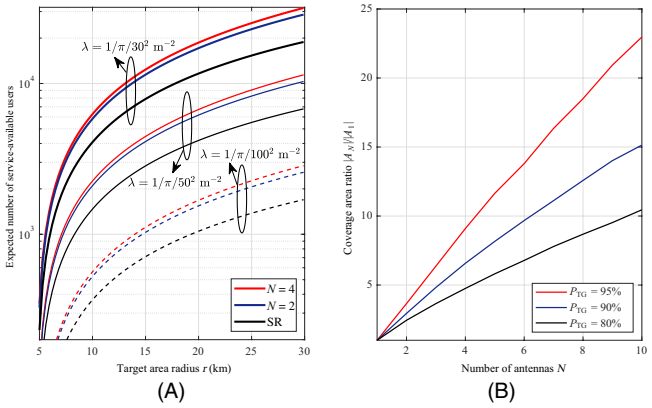

FIGURE 6 (A) Expected number of service-available users vs. target area radius, (B) $|\mathscr{A}_N|/|\mathscr{A}_1|$ vs. N under the Hata path-loss model (Noise Level −90 [dBm], $\epsilon_{th} = 5$ [dB], $v = 80$ [km/h], $f_c = 600$ [MHz], $T_s = 1/419$ [s], $P_T = 47.6336$ [dBm], $r_0 = 5$ [km], $h_T = 200$ [m], $h_R = 2$ [m], $C_m = 0$ [dB])

with a density κ. Figure 6A compared $n_N(r)$ for MR and SR with respect to r. One can see that the $n_N(r)$ gain obtained from installing a single additional antenna to an SR was significant, whereas that obtained by doubling the N of a two-antenna MR was relatively small. However, according to the results in Figure 6B, the coverage area extension itself was proportional to N and the expansion was further substantial under more rigorous p_{TG} constraints.

6 | FIELD EXPERIMENT RESULTS

6.1 | Test environment description

Empirical results of the mobile field measurements were also obtained to verify the MR gain in practice. The Tx facilities used for the mobile field trials were installed at Jeju Techno Park, Jeju Island, Republic of Korea. The Tx site was located 357 m above the vertical datum (sea level), and had additional building and antenna heights of 16 m and 5 m, respectively. ATSC 3.0 radio signals, which contain an audio/video (A/V)-carrying media stream, were transmitted over the air via Channel 50 (689 MHz), where the transmission power was 500 W effective isotropic radiated power with a 50 W high-power amplifier output and 10 dB antenna gain. To elaborate, the transmission chain, which consists of an audio/video stream live encoder, an Internet Protocol (IP) stream multiplexer, a broadcast gateway, and an exciter, which is fully compliant with ATSC 3.0 standards, for example, A/321, A/322, and A/324, was used for the experiments.

Figure 2 abstractly depicts the configuration of the field trials. For the Rx-side, the measurements were conducted within a test vehicle that has four receive antennas mounted on its rooftop. A 1.9 m × 5.1 m × 1.9 m-size utility van customized for radio frequency (RF) field measurements was used for the testing. More precisely, the antennas were deployed in a rectangular topology 1.5 m in width and 1.7 m in length. At the center of the antenna arrangement, a Global Positioning System (GPS) antenna for vehicle tracing was installed. Note that the wavelength of the 689 MHz wave ($\triangleq \lambda_{689}$) is about 0.435 m, and every antenna-by-antenna distances was set to be greater than $\lambda_{689}/2$ to prevent resonant coupling among the antennas. Inside the test vehicle, a prototype MR, implemented to perform MRC for up to four RF signal inputs (refer to Figure 7), was installed along with a spectrum analyzer, A/V decoder, and a GPS receiver. These components were integrated into a cooperative, and GPS-synchronized, measurement/analysis system managed by a dedicated software-based control. Measurements were conducted in real time through 0–100 km/h drives over the urban and suburban regions of Jeju City, Rep. of Korea. The measurement data were combined with the synchronized GPS metadata to indicate the reception successes and failures at each location across the test route, point-by-point, where the GPS positioning data were acquired in one second intervals.

6.2 | MR Gain Verification

To evaluate the MR gain in the experiments, a 16 non-uniform constellation (NUC)-mapped, 6/15-rate low-density parity check (LDPC)-coded, and 16K fast Fourier transform (FFT)-modulated ATSC 3.0 physical layer signal was transmitted, as described in Table 1. A 1080p FHD video was conveyed in the transmission, and the transmission configured by Table 1 was physically capable of delivering 7.79 Mbps and had a

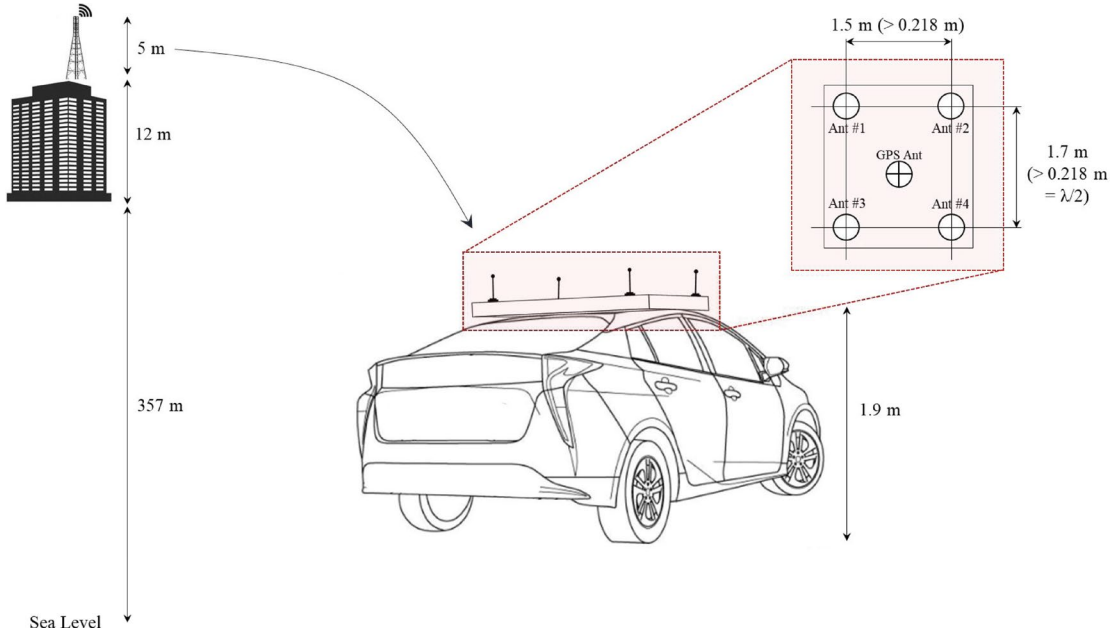

FIGURE 7 The schematic illustration of mobile field trials

4.56 dB ToV in an additive white Gaussian noise (AWGN) channel [37].

It can be graphically found in Figure 8 that the MR substantially reduces the reception failures in mobile environments.[2] For the sake of clarity, each of the reception success and failure points is indicated by green and black markers, respectively. Focusing on the north side of the subfigures, which was the furthest area from the Tx within the test route and was also shadowed by terrain features, the use of additional receive antennas explicitly converted more reception failure points into reception success points. Moreover, the SR reception failure points located on the south side of the test route, which arose from several obstacles, such as buildings and hilly areas, were successfully covered by the use of multiple antennas, which demonstrated the effectiveness of MR in practice.

The field test results were more precisely investigated through ESR5 curve analysis. Using the ITU-R recommendation, the portion of successful reception points out of the total measurement points, the so-called *successful reception rate*, is plotted in Figure 9. It should be noted that while the successful reception rate is an empirical term, it can be translated into the coverage probability from previous sections. Observed in Figure 9, the $N = 4$ MR achieved the 7 dB required signal strength gain for 95 % coverage probability compared to the SR. If we simulate on the basis of the Hata model and assume that a signal strength of -80 dBm appears at $r = 1.3$ km, then the impact of this 7 dB gain translates into a 315% increase in coverage area compared to the SR. This result may be highly encouraging for network enablers, since a coverage area expansion could allow seamless mobile services of FHD within legacy infrastructures. In other words, the capital and operating expenditures (CAPEX and OPEX) required for seamless mobile broadcasting can be significantly reduced by distributing MR on vehicles.

6.3 | MR Performance under LDM and TDM Transmissions

Additional brief experiments were conducted to verify the mobile MR performance under LDM, particularly based on the configuration in Table 2. Each physical layer parameter configuration was denoted by $\mathcal{S}_{\text{sgl}}$, $\mathcal{S}_{\text{TDM}}$, and $\mathcal{S}_{\text{LDM}}$, where $\mathcal{S}_{\text{sgl}}$ and $\mathcal{S}_{\text{TDM}}$ correspond to TDM scenarios and $\mathcal{S}_{\text{LDM}}$ stands for LDM transmission.[3] We specifically focused on the mobile delivery of UHD contents at near-20 Mbps bit rates. To ensure a fair comparison, $\mathcal{S}_{\text{TDM}}$ was configured to have two different subframes in each frame, where the 2nd subframe was defined to have a throughput analogous to the EL of $\mathcal{S}_{\text{LDM}}$. Correspondingly, the EL of $\mathcal{S}_{\text{LDM}}$, the 2nd subframe of $\mathcal{S}_{\text{TDM}}$, and $\mathcal{S}_{\text{sgl}}$ were compared. Therefore, a comparison was conducted between the LDM EL and the corresponding TDM subframe modulated by high-order constellation mapping.

[2]Although experiments for different $$N$$ s were not carried out simultaneously, every selected trial was heuristically controlled to secure the same reception environment to each other as possible.

[3]To be exact, $\mathcal{S}_{\text{sgl}}$ is not a TDM transmission because it consists of a single PLP in each frame. However, the reception performances of single PLP and TDM transmissions are identical to each other, and hence we comprehensively refer to the $\mathcal{S}_{\text{sgl}}$ result as a TDM performance.

TABLE 1 ATSC 3.0 physical layer configuration for field tests - MR diversity gain verification

Frame Length (Symbol-Aligned)		255.33 ms
Occupied Bandwidth		5.832844 MHz
Bootstrap Sample Length		1/6.144 us
Bootstrap Carrier Spacing		3 kHz
Preamble/Payload Sample Length		1/6.912 us
Preamble/Payload Carrier Spacing		421.875 Hz
Preamble Parameters	FFT Size	16K
	Guard Interval	148.148 us (GI5_1024)
	Pilot Pattern	SP Dx = 3
	Signaling Protection	L1-Basic Mode 1
	# of Preamble Symbols	1
Payload OFDM Parameters	FFT Size	16K
	Guard Interval	148.148 us (GI5_1024)
	Pilot Pattern	SP6_2 (Dx = 6, Dy = 2)
	Pilot Boosting	1 (1.202 dB)
	# of Payload Symbols	98
	Time Interleaver	CTI Depth of 1024
	Frequency Interleaver	On
	Subframe Boundary Symbol	First: On, Last: On
Payload BICM Parameters	Outer Code	BCH
	Inner Code	6/15 LDPC (64 800 bits)
	Constellation	16 NUC
Data rate		7.79 Mbps
Required C/N (AWGN)		4.56 dB

As detailed in Table 2, the service rates of interest in $\mathcal{S}_{\text{sgl}}$, $\mathcal{S}_{\text{TDM}}$, and $\mathcal{S}_{\text{LDM}}$ were 26 Mbps, 20.18 Mbps, and 20.46 Mbps, respectively. The corresponding ToVs of $\mathcal{S}_{\text{sgl}}$, $\mathcal{S}_{\text{TDM}}$, and $\mathcal{S}_{\text{LDM}}$ measured in the AWGN channel were 15.87 dB, 17.86 dB, and 19.59 dB, respectively.

The field test results for the LDM/TDM comparison with mobile MRs are illustrated in Figure 11. As visualized by the green and black markers, $\mathcal{S}_{\text{sgl}}$ yielded an obviously worse reception performance than the others, while $\mathcal{S}_{\text{TDM}}$ and $\mathcal{S}_{\text{LDM}}$ were found to have similar coverage. This performance degradation of $\mathcal{S}_{\text{sgl}}$ was mainly due to the use of a larger FFT size. Large FFTs yield narrow subcarrier spacings, leading to high ICI levels, which make the waveforms fragile to mobility (see [11], [19] and therein). Given the concern of the vulnerability of large-size FFT to mobility, the physical layer guideline for ATSC 3.0 [12], does not recommend the use of a 32K FFT for mobile services. Note also that $\mathcal{S}_{\text{TDM}}$ can achieve up to 27.65 Mbps when the 1st subframe is removed, which implies that $\mathcal{S}_{\text{TDM}}$ provides even more throughput than $\mathcal{S}_{\text{sgl}}$. As

FIGURE 8 Experiment environment description: Prototype MR implementation (upper-left), real-time signal analysis within the test vehicle (upper-right), and antenna installation at the test vehicle (bottom)

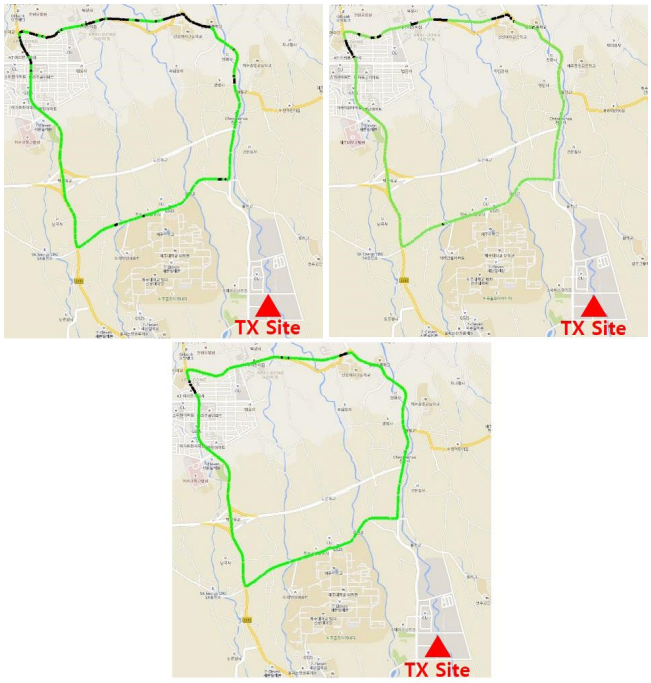

FIGURE 9 Reception success and failure points over the testing route: Reception success (green), reception failure (black). SR (upper-left), MR with $N = 2$ (upper-right), and MR with $N = 4$ (bottom)

for the practice of ATSC 3.0, our result in Figure 7 could accordingly contribute as an example that justifies the omission of 32K-FFT from ATSC 3.0 mobile service profiles.

Besides, the analogous performances of $\mathcal{S}_{\text{TDM}}$ and $\mathcal{S}_{\text{LDM}}$ are encouraging since the LDM CL served 2.28 Mbps more

TABLE 2 ATSC 3.0 physical layer configuration for LDM/TDM comparison tests

Scenario		$\mathcal{S}_{sgl}$	$\mathcal{S}_{TDM}$	$\mathcal{S}_{LDM}$
Frame Length (Symbol-Aligned)		354 ms	185.85 ms	
Occupied Bandwidth		5.832 844 MHz		
Bootstrap Sample Length		1/6.144 us		
Bootstrap Carrier Spacing		3 kHz		
Preamble/Payload Sample Length		1/6.912 us		
Preamble/Payload Carrier Spacing		210.9375 Hz	421.875 Hz	
Preamble Parameters	FFT Size	32K	16K	
	Guard Interval	148.148 us (GI5_1024)		
	Pilot Pattern	SP Dx = 12	SP Dx = 6	
	Signaling Protection	L1-Basic Mode 3	L1-Basic Mode 1	
	# of Preamble Symbols	1		
Payload OFDM Parameters	FFT Size	32K	16K	
	Guard Interval	148.148 us (GI5_1024)		
	Pilot Pattern	SP24_2 (Dx = 24, Dy = 2)	SP12_4 (Dx = 12, Dy = 4)	
	# of Payload Symbols	71	Sub1: 19, Sub2: 53	60
	Time Interleaver	CTI Depth of 1024		
	Frequency Interleaver	On		
	Subframe Boundary Symbol	First: On, Last: On		
	Injection Level	N/A		-5 dB
Payload BICM Parameters	Outer Code	BCH		
	Inner Code	9/15 LDPC	Sub1: 10/15, Sub2: 8/15 LDPC	CL: 6/15, EL: 10/15 LDPC
	Constellation	256 NUC	Sub1: QPSK, Sub2: 1k NUC	CL: QPSK, EL: 64 NUC
Data rate		**26 Mbps**	Sub1: 1.80 Mbps, **Sub2: 20.18 Mbps**	CL: 4.08 Mbps, **EL: 20.46 Mbps**
Required C/N (AWGN)		**15.87 dB**	Sub1: 3.07 dB, **Sub2: 17.86 dB**	CL: 2.85 dB, **EL: 19.59 dB**

data than the 1st subframe of $\mathcal{S}_{TDM}$. According to Section 4.2, LDM EL does not provide additional tolerability to ICI. Further, $\mathcal{S}_{LDM}$ yielded slightly more reception failures because $\mathcal{S}_{LDM}$ was originally configured to have a higher ToV than $\mathcal{S}_{TDM}$ in the AWGN channel. Nevertheless, the result in Figure 10 implies that the efficient framing feature of LDM (particularly for unequal error protection scenarios with multiple services) could offer better EL mobile performance than TDM if the bit-interleaved coded modulation (BICM) configuration is properly adjusted for mobile UHD purposes.

7 | CONCLUSION

This study analyzed the reliability gain that can be obtained by using multiple antennas in mobile broadcasting Rxs mounted on vehicles. The advantages of MR over SR were verified in terms of coverage probability, particularly as a function of the ratio between the ToV and field strength. Analytical derivations revealed that MR achieves significantly better coverage probability than SR, especially under harsh conditions with low ergodic field strengths and high SINR requirements. These results were carefully extended to discover the gains in terms of geometric coverage and served-user volume. To incorporate the practical transmission scenarios with multiple services in a single RF band, the mobile reliability gain of LDM was additionally examined through comparisons with TDM on top of our framework. Moreover, the field measurement results obtained from the on-air ATSC 3.0 broadcast transmissions demonstrated that MR with a few more antennas achieves notable reliability gain over SR. Specifically, compared to the field strength requirements of SR, a field strength of approximately 7 dB less was required for a four-antenna MR to guarantee a 95% ESR for a 7.79 Mbps FHD service. Owing to the

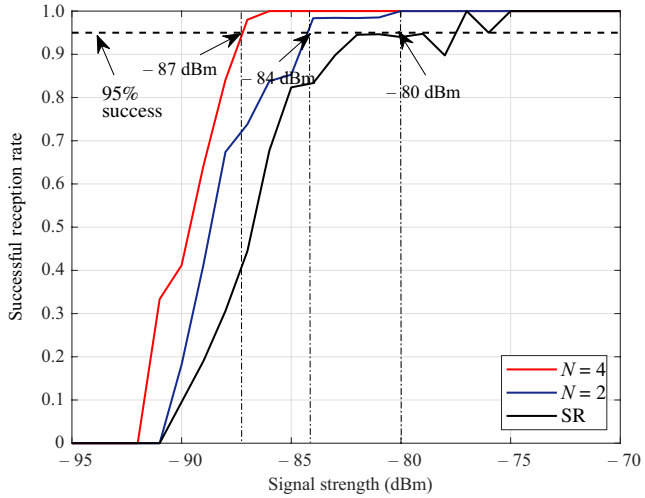

FIGURE 10 Field experiment results: Successful reception rate vs. signal strength (ESR curves)

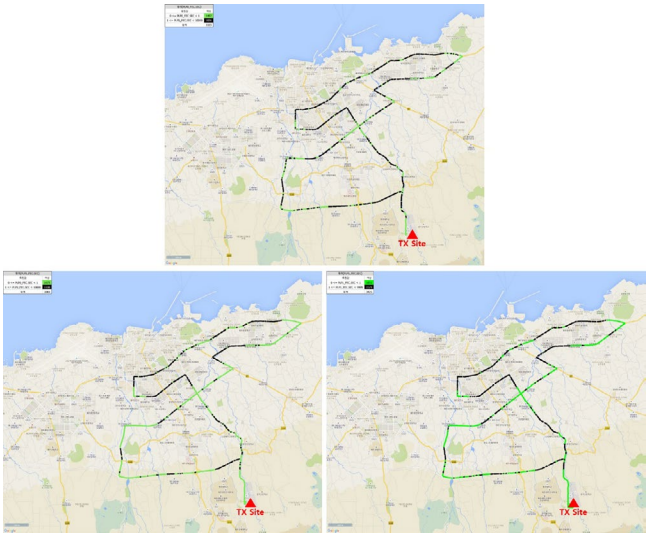

FIGURE 11 Reception performance comparison among the TDM and LDM scenarios: Reception success (green), reception failure (black). $\mathcal{S}_{\text{sgl}}$ (upper), $\mathcal{S}_{\text{TDM}}$ (lower left), and $\mathcal{S}_{\text{LDM}}$ (lower right)

substantial tolerability gain against Rx mobility, MR was verified to be a convincing solution for distributing mobile FHD/UHD broadcasts in the future automotive era.

ORCID

Sungjun Ahn https://orcid.org/0000-0003-2933-5528

REFERENCES

1. S.-I. Park et al., *Mobile performance of diversity receiver in ATSC 3.0 system*, in Proc. IEEE Int. Symp. Broadband Multimed. Syst. Broadcast. (Paris, France), June 2020, pp. 1–3.
2. J. Lee et al., *IP-based cooperative services using ATSC 3.0 broadcast and broadband*, IEEE Trans. Broadcast. **66** (2020), 440–448.
3. S. Ahn et al., *Mobile performance enhancement via tracking inter-carrier interference power for ATSC 3.0 receivers*, in Proc. IEEE Int. Symp. Broadband Multimed. Syst. Broadcast. (Paris, Fance), June 2020.
4. S. Ahn et al., *Cooperation between LDM-based terrestrial broadcast and broadband unicast: On scalable video streaming applications*, IEEE Trans. Broadcast. **67** (2021), no. 1, 2–22.
5. S. Ahn et al., *Fronthaul compression and precoding optimization for NOMA-based joint transmission of broadcast and unicast services in C-RAN*, IEEE Trans. Broadcast. **66** (2020), no. 4, 786–799.
6. L. Zhang et al., *Using non-orthogonal multiplexing in 5G-MBMS to achieve broadband-broadcast convergence with high spectral efficiency*, IEEE Trans. Broadcast. **66** (2020), 490–502.
7. H.-H. Liu and H.-Y. Wei, *Towards NR MBMS: A flexible partitioning method for SFN areas*, IEEE Trans. Broadcast. **66** (2020), 416–427.
8. E. Iradier et al., *Using NOMA for enabling broadcast/unicast convergence in 5G networks*, IEEE Trans. Broadcast. **66** (2020), 503–514.
9. T. Tran et al., *Enabling multicast and broadcast in the 5G core for converged fixed and mobile networks*, IEEE Trans. Broadcast. **66** (2020), 428–439.
10. D. Gomez-Barquero et al., *IEEE transactions on broadcasting special issue on: Convergence of broadcast and broadband in the 5G era*, IEEE Trans. Broadcast. **66** (2020), 383–389.
11. S. Ahn et al., *Mobile performance evaluation for ATSC 3.0 physical layer modulation and code combinations under TU-6 channel*, to be published in IEEE Trans. Broadcast. **66** (2020), no. 4, 752–769.
12. Advanced Television Systems Committee, ATSC Recommended Practice: A/327, Guidelines for the Physical Layer Protocol, Doc. A/327, Oct. 2018.
13. S.-K. Ahn et al., *Comparison of low-density parity-check codes in ATSC 3.0 and 5G standards*, IEEE Trans. Broadcast. **65** (2019), 489–495.
14. L Michael and D. Gamez-Barquero, *Bit-interleaved coded modulation (BICM) for ATSC 3.0*, IEEE Trans. Broadcast., Mar. **62** (2016), 181–188.
15. K.-J. Kim et al., *Low-density parity-check codes for ATSC 3.0*, IEEE Trans. Broadcast. **62** (2016), 189–196.
16. J. Barrueco et al., *Constellation design for bit-interleaved coded modulation (BICM) systems in advanced broadcast standards*, IEEE Trans. Broadcast. **63** (2017), 603–614.
17. S. Ahn et al., *Large-scale network analysis on NOMA-aided broadcast/unicast joint transmission scenarios considering content popularity*, IEEE Trans. Broadcast. **66** (2020), no. 4, 770–785.
18. E. Garro et al., *5G mixed mode: NR multicast-broadcast services*, IEEE Trans. Broadcast. **66** (2020), 390–403.
19. Y. Li and L. J. Cimini, *Bounds on the interchannel interference of OFDM in time-varying impairments*, IEEE Trans. Commun. **49** (2001), 401–404.
20. D. Gomez-Barquero et al., *DVB-NGH: The next generation of digital broadcast services to handheld devices*, IEEE Trans. Broadcast. **60** (2014), 246–257.
21. Z. Niu et al., *A new paradigm for mobile multimedia broadcasting based on integrated communication and broadcast networks*, IEEE Commun. Mag. **46** (2008), 126–132.
22. M. R. Chari et al., *FLO physical layer: An overview*, IEEE Trans. Broadcast. **53** (2007), 145–160.
23. I. Chatzigeorgiou, *Bounds on the lambert function and their application to the outage analysis of user cooperation*, IEEE Commun. Lett. **17** (2013), 1505–1508.

24. The ESR5 Criterion for the Assessment of DVB-T Transmission Quality, document 6E/64-E, ITU-R, Geneva, Switzerland, Apr. 2004.
25. S.-I. Park et al., *Field comparison tests of LDM and TDM in ATSC 3.0*, IEEE Trans. Broadcast. **64** (2018), 637–647.
26. A. Adhikary et al., *Joint spatial division and multiplexing: The large-scale array regime*, IEEE Trans. Inf. Theory **59** (2014), 6441–6463.
27. A. Forenza, D. J. Love, and R. W. Heath, *Simplified spatial correlation models for clustered MIMO channels with different array configurations*, IEEE Trans. Veh. Technol. **56** (2007), 1924–1934.
28. J. Montalban et al., *Cloud transmission: System performance and application scenarios*, IEEE Trans. Broadcast. **60** (2014), 170–184.
29. S. Kwon et al., *Detection schemes for ATSC 3.0 transmitter identification in single frequency network*, IEEE Trans. Broadcast. **66** (2020), 229–240.
30. J. Lee et al., *Transmitter identification signal detection algorithm for ATSC 3.0 single frequency networks*, IEEE Trans. Broadcast. **66** (2020), 737–743.
31. S.-I. Park et al., *Low complexity layered division multiplexing for ATSC 3.0*, IEEE Trans. Broadcast. **62** (2016), 233–243.
32. L. Zhang et al., *Layered-division-multiplexing: Theory and practice*, IEEE Trans. Broadcast. **62** (2016), 216–232.
33. L. Zhang et al., *Using layered-division-multiplexing to deliver multi-layer mobile services in ATSC 3.0*, IEEE Trans. Broadcast. **65** (2019), 40–52.
34. C. Regueiro et al., *LDM core services performance in ATSC 3.0*, IEEE Trans. Broadcast. **62** (2016), 244–252.
35. Advanced Television Systems Committee, ATSC Standard: A/322, Physical Layer Protocol, Doc. A/322, Jun. 2017.
36. E. Damosso, *Digital mobile radio: Towards future generation systems*, European Commission, Final Report of the COST 231 Project. Chapter 4. 1998.
37. S.-I. Park et al., *Performance analysis for all modulation and code combinations of ATSC 3.0 physical layer protocol*, IEEE Trans. Broadcast. **64** (2019), no. 2, 197–210.

AUTHOR BIOGRAPHIES

Sungjun Ahn received his BS and MS degrees in electrical engineering from the Korea Advanced Institute of Science and Technology, Daejeon, Rep. of Korea, in 2015 and 2017, respectively. He has been with the Media Transmission Research Group, Electronics and Telecommunications Research Institute, since 2017, where he is currently a research engineer. He has authored more than 40 technical publications in peer-reviewed journals and conference proceedings. His research interests include stochastic geometry analysis, signal processing, and optimization for wireless communications and digital broadcasting.

Jae-young Lee received his BS degree (High Hons.) in electrical and computer engineering from Rutgers University in 2001, his MS degree in electrical and computer engineering from the University of Wisconsin at Madison in 2003, and his PhD degree in Engineering Science from Simon Fraser University in 2013. He joined the Electronics and Telecommunications Research Institute (ETRI) in 2003 and is currently a principal research associate at the Broadcasting Systems Research Group of ETRI. His research interests are in the areas of digital signal processing for various applications, including digital broadcasting, telecommunications, and human-computer interaction systems.

Bo-Mi Lim received her BS degree from Ajou University, Suwon, Rep. of Korea, in 2008 and her MS degree from the Korea Advanced Institute of Science and Technology, Daejeon, Rep. of Korea, in 2010. Since 2010, she has been a member of the research staff at the Media Research Division, Electronics and Telecommunications Research Institute. Her research interests are in the areas of wireless communication system design and digital broadcasting.

Hae-Chan Kwon received his BS and MS degrees from the Korea Maritime and Ocean University, Busan, Rep. of Korea, in 2013 and 2015, respectively. Since 2015, he has been with the Media Research Division, Electronics and Telecommunications Research Institute as a member of research staff. His research interests are in the areas of wireless communication system design and digital broadcasting.

Namho Hur received his BS, MS, and PhD degrees in electrical and electronic engineering from the Pohang University of Science and Technology, Pohang, Rep. of Korea, in 1992, 1994, and 2000, respectively. He is currently with the Broadcasting and Media Research Laboratory, Electronics and Telecommunications Research Institute, Daejeon, Rep. of Korea, where he is the project leader of "Development of Transmission Technology for Ultra High Quality UHD." He was the chair of the Future of Broadcast Television Initiative Management Committee from April 2018 to April 2019. His research interests include realistic digital broadcasting systems.

Sung-Ik Park received his BSEE degree from Hanyang University, Seoul, Rep. of Korea, in 2000, his MSEE degree from POSTECH, Pohang, Rep. of Korea, in 2002, and his PhD degree from Chungnam National University, Daejeon, Rep. of Korea, in 2011. Since 2002, he has been with the Broadcasting System Research Group, Electronics and Telecommunication Research Institute (ETRI), where he is the project leader and principal member of research staff. His research interests are in the area of error correction codes and digital communications, in particular, signal processing for digital television. He has over 200 peer-reviewed journal and conference publications, and multiple best paper and contribution awards for his work on broadcasting technologies. He currently serves as an associate editor for the *IEEE Transactions on Broadcasting* and *ETRI Journal* and is a distinguished lecturer of the IEEE Broadcasting Technology Society.